energies

Article

Well-Logging Constraints on Gas Hydrate Saturation in Unconsolidated Fine-Grained Reservoirs in the Northern South China Sea

Xiaoming Wan [1,2], Xueqing Zhou [3,*], Jinqiang Liang [2], Shiguo Wu [3], Jingan Lu [2], Chenglong Wei [1,2], Rui Wang [1] and Bo Liu [4,*]

1 Haikou Marine Geological Survey Center, Chinese Geological Survey, Haikou 571127, China
2 Key Laboratory of Marine Mineral Resources, Ministry of Natural Resources, Guangzhou Marine Geological Survey, China Geological Survey, Guangzhou 510075, China
3 Laboratory of Marine Geophysics and Georesources, Institute of Deep-Sea Science and Engineering, China Academy of Sciences, Sanya 572000, China
4 School of Earth Science and Engineering, Hebei University of Engineering, Handan 056038, China
* Correspondence: zhouxq@idsse.ac.cn (X.Z.); liubo@hebeu.edu.cn (B.L.)

Abstract: Recently, drilling wells have encountered rich gas hydrates in fine-grained sediments in the northern South China Sea. Gas hydrate in fine-grained sediments is very heterogeneous, and its physical properties are different from those of oil and gas reservoirs. The reliability of the classical logging saturation evaluation models established for diagenetic reservoirs is questionable. This study used four wells in GMGS3 and GMGS4 to evaluate the effects of the application of three typical methods for evaluating saturation with different principles in the unconsolidated fine-grained sediments: nuclear magnetic logging, sigma logging, and the Archie formula. It was found that the value of the lithologic capture cross-section in sigma logging and the rock's electrical parameters in the Archie formula affect the accuracy of the model. Therefore, to obtain a reliable saturation value for fine-grained sediments, an innovative method for the calculation of resistivity and acoustic time is proposed to estimate gas hydrate saturation based on logging data, which is most consistent with the results of core analysis. The overall relative error of the verification well was 5.87%, whereas that of the density NMR logging method was 56%, showing that the accuracy of the newly proposed resistivity DT logging method's saturation formula was significantly improved. Finally, a new model-based cross chart was developed, which can rapidly differentiate gas saturation during drilling.

Keywords: gas hydrates; well log; gas hydrate saturation; resistivity and acoustic time calculation method; South China Sea

Citation: Wan, X.; Zhou, X.; Liang, J.; Wu, S.; Lu, J.; Wei, C.; Wang, R.; Liu, B. Well-Logging Constraints on Gas Hydrate Saturation in Unconsolidated Fine-Grained Reservoirs in the Northern South China Sea. *Energies* **2022**, *15*, 9215. https://doi.org/10.3390/en15239215

Academic Editors: Taohua He, Junqian Li and Wenhao Li

Received: 25 October 2022
Accepted: 30 November 2022
Published: 5 December 2022

1. Introduction

Gas hydrates are ice-like solid substances composed of water and natural gas. They are formed under low temperatures, high pressure, and appropriate gas concentrations [1]. Gas hydrates are widely distributed in the continental margin and are potential clean energy resources [2,3]. According to 20 years of exploration, gas hydrates are widely distributed in the northern South China Sea [4–7]. Bottom-simulating reflectors (BSRs) have usually been considered to be an indicator of gas hydrates [8–10]. In addition, BSRs have been regarded as the bottom boundary of the gas hydrate stability zone (GHSZ) [11]. Full-waveform pre-stack inversion was applied to calculate P-velocity, S-velocity, and density in the Gulf of Mexico. Then, gas hydrate saturation was estimated from P-wave impedance (the product of velocity and bulk density) using rock physics models [12,13]. However, the resolution of the evaluation cannot satisfy the needs of gas hydrate development.

Well logs can provide good-quality parameters for gas hydrate saturations [14]. Various theoretical and semi-empirical models have been proposed to estimate gas hydrate saturation. At present, the calculation of gas hydrate reservoir saturation follows the method for conventional evaluation of reservoir saturation logging [15–18]. The existence of gas hydrates in sediments significantly affects their physical properties—especially resistivity logging and acoustic logging, which are among the most sensitive measurements for the existence of gas hydrates.

The commonly used method of using resistivity logging curves is based on the classical Archie model [19]. The classical Archie formula was proposed based on pure sandstone reservoirs with medium and high porosity, mainly intergrain pores, unimodal pore distribution, and good pore–throat matching [20]. The key parameters include a, b, m, and n [21]. Based on gas hydrate data in different regions, many scholars have conducted multi-angle and multidirectional research on the calculation and evaluation of the electric parameters of the rocks and calculated gas hydrate reservoir saturation [22]. However, there are still some problems in applying the Archie formula in gas hydrate reservoirs. Firstly, it is difficult to obtain the electrical parameters of the rocks. Compared with conventional reservoirs, it is challenging to carry out electrical experiments on rocks in unconsolidated sediments. Due to a lack of attention to the core physical properties of experiments in sediment drilling, it is difficult to obtain the electrical parameters of the rocks, which constitutes the biggest problem in the calculation of saturation at present. Secondly, the petroelectric characteristics of hydrate-bearing sediments are quite different from those of conventional petrogas-bearing rocks. The distribution form of hydrates affects their conductivity, leading to the "non-Archie" phenomenon. Thirdly, the difference in sediment rock composition affects the accurate application of the Archie model, especially in sediments with high clay content [23]. Faced with the difficulties in the application of the Archie formula in gas hydrate reservoirs, a series of modified and alternative models have gradually been developed [24,25]. Confronted with the difficulty of obtaining the electrical parameters of the rocks through experiments, the use of the logging resistivity value of the water-sediment layer without gas hydrate as the benchmark has been proposed to calculate the electrical parameters of the rocks [26]. For gas-hydrate-bearing reservoirs, a variable-parameter Archie model specifically applicable to the target block has also been proposed [27,28]. At the same time, the additional conductive effect of clay has been studied [29].

Saturation models based on acoustic logging in gas hydrate reservoirs have also been proposed. Many acoustic log analysis models—such as the Wood equation, as well as rock physics models such as the effective medium theory, Biot–Gassmann theory, three-phase Biot theory, and time-averaged equations [30,31]—have been used to derive gas hydrate saturations using compressional wave velocities. Moreover, considering both pore-filling and fracture-filling acoustic reservoir models, an acoustic logging evaluation model for gas hydrate content has been established [32].

In addition to the application of the Archie model and acoustic models, scholars have proposed new saturation calculation methods, including the density NMR logging method and sigma logging formula, based on various petrophysical models [3,33]. However, relevant research is mainly based on basic rock physics, leading to most of the current logging-based petrophysical models of hydrate reservoirs being applicable to conventional diagenetic oil and gas reservoirs, which are very different from hydrate reservoirs. Therefore, the physical response of hydrate reservoirs with deep-sea sedimentary characteristics must be considered. With the deepening of hydrate exploration, more and more types of hydrate reservoirs have been found. For fine hydrate reservoirs with strong heterogeneity, the quality difference between reservoirs is large, and the effectiveness, applicable conditions, and limitations of various saturation calculation methods in unconsolidated gas hydrate (GH) reservoirs (e.g., diagenetic, argillaceous, silty) have not been fully discussed [34]. Accordingly, based on logging data and core analysis data, this paper compares the applicable conditions and limitations of evaluation methods such as nuclear magnetic logging, the Archie formula, and the sigma logging formula. Furthermore, we propose an innovative method for calculating resistivity and acoustic time and establish a quick chart for judging hydrates saturation. This is helpful for real-time evaluation and judgment in the logging-while-drilling (LWD) process and for improving the accuracy of saturation interpretation.

In this paper, we apply well-logging evaluation methods to estimate the GH saturation in fine-grained sediments. Four kinds of well-logging methods—nuclear magnetic logging, sigma logging, the Archie formula, and resistivity and acoustic time calculation—are discussed, including their applicable conditions and limitations.

2. Geological Setting

The slope of the passive continental margin is a gas hydrate domain. Tectonically, it belongs to the Baiyun Depression of the Pearl River Mouth Basin (Figure 1a). In terms of geomorphology, the deep-water canyons, valleys, ridges, gullies, and slides are well-developed on the slope of the South China Sea. The overall trend of the submarine canyon is from north to south, and the water gradually deepens from 1000 m to more than 1700 m. In the north of the drilling area, three nearly north–south submarine valleys run from west to east. Drilling wells are located at north–south striking submarine ridges (Figure 1b).

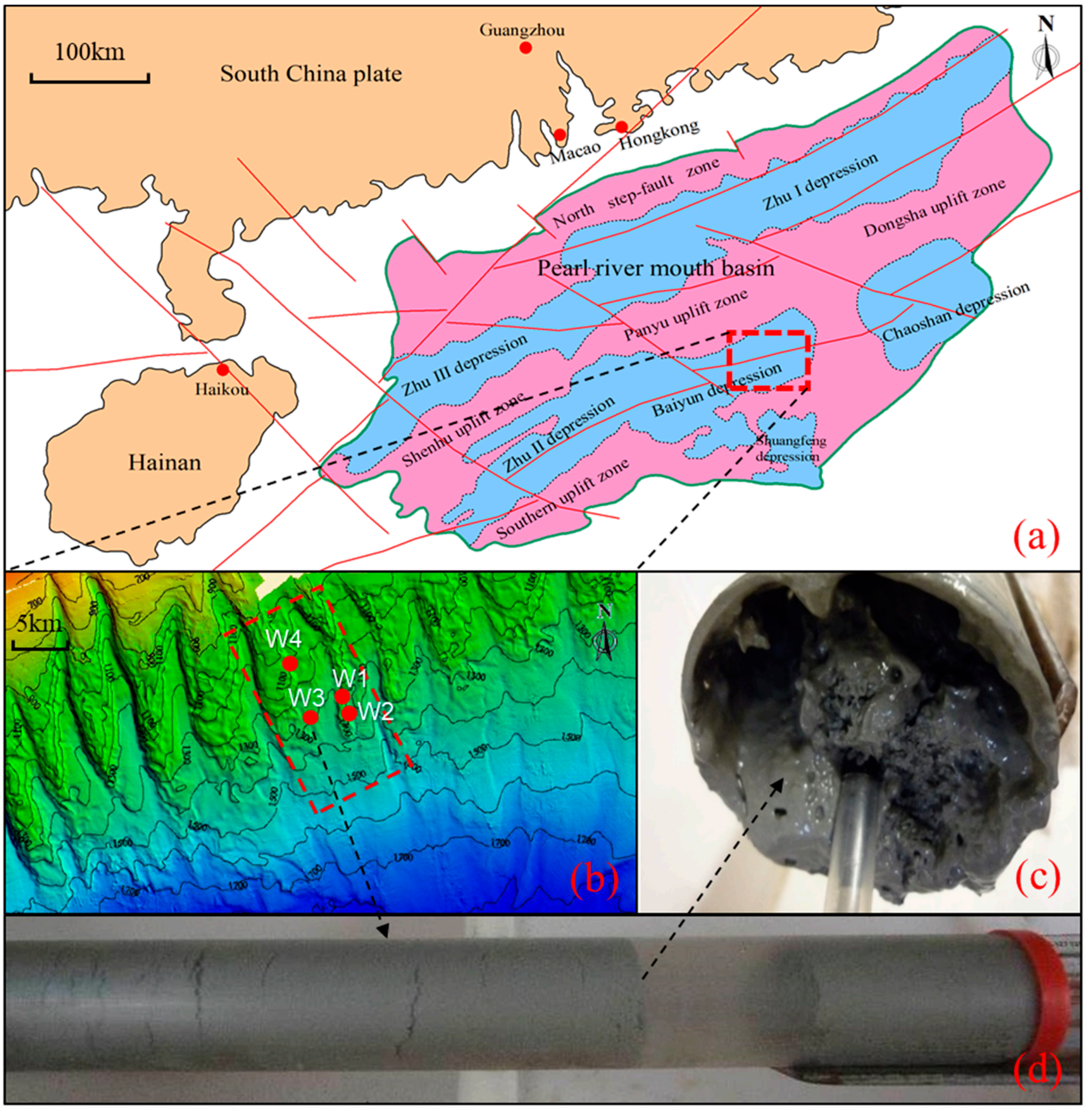

Figure 1. (**a**) Tectonic position of the Pearl River Mouth Basin. (**b**) Geomorphology and well position in the gas hydrate drilling cruises in study area (red rectangle). (**c**) Gas hydrate reservoirs in the unconsolidated fine-grained sediments (**d**) Unconsolidated fine-grained sediments.

From the Middle Miocene to the Quaternary, the whole Pearl River Mouth Basin entered a differential thermal subsidence stage. With the cessation of the sea floor's spread in the South China Sea, the Pearl River Mouth Basin tilted to the south, and the marine invasion intensified. The whole Pearl River Mouth Basin became a wide sea-shelf sedimentary environment. The Pearl River Mouth Depression, where the study area is located, became the subsidence center of the Pearl River Mouth Basin, forming a set of shallow-sea–bathyal facies fine sediments. Gas hydrates occurred in the unconsolidated fine-grained sediments (Figure 1c). Grain size analysis shows that the sediments in the drilling hole are mainly clayey siltstone and siltstone. Moreover, the mineral content in the quantitative analysis report of the whole-rock X-ray diffraction includes sandstone, carbonate rock, clay, etc. (Figure 1d). The results of the chemical composition analysis of the sediment from each core show that the chemical composition of the sediment is dominated by SiO_2, Al_2O_3, and marine biological carbonate ($CaCO_3$), representing terrestrial input. The distribution trend of chemical components indicates that the study area was dominated by the input of terrigenous materials from the Late Miocene to the Early Pliocene [35], and the marine carbonate deposition was relatively low. In the Early Pliocene, the input of terrigenous materials decreased and carbonate deposits developed relatively quickly. In the Late Pliocene, and especially since the Pleistocene, the sediment sources showed obvious characteristics of terrigenous input and biological carbonate alternation. Due to the low contents of other minerals (pyrite, hematite, gypsum, etc.), the lithological composition of the Shenhu area can be simplified to sandstone, carbonate rock, and clay [36].

GH reservoirs in the study area vary greatly, as the sedimentary facies varies from mass transport deposits to turbidites, to hemipelagic sediments. The gas-hydrate-bearing formations are loose and highly porous. Existing interpretation results are limited to evaluating the physical properties of gas hydrate reservoirs in a single well, and the evaluation method still follows the previous evaluation model and theory of oil and gas reservoirs. This study aims to establish an evaluation method for gas hydrate reservoir parameters based on geological characteristics and core experimental data.

3. Data and Methods

3.1. Data

The LWD data were acquired during GMGS3 and GMGS4—two gas hydrate expedition cruises in 2015 and 2016, respectively [37–39]. GMGS3 and GMGS4 drilled three wells and one well, respectively. Wells W1, W2, and W3 were drilled during GMGS3, while Well W4 was drilled during GMGS4 (Figure 1b). These four drilling sites all include pilot holes and core holes. The pilot hole's LWD process mainly obtains resistivity, acoustic wave, density, neutron, and gamma-ray logging data while drilling and it monitors resistivity, acoustic wave, and gamma-ray logging in real-time. Other logs include borehole diameter, acoustic full-wave train, resistivity imaging logs, and NMR spectrum data, which determine the target station and target horizon for subsequent gas hydrate drilling and coring.

All of the above four pilot wells have good logging data, with none missing except for NMR logging data (Figure 2). The gamma, resistivity, neutron density, and acoustic wave measurements obtained using NeoScope are affected by the expansion of the upper zone's diameter. Overall, the data quality of these wells is good and meets the needs of interpretation (Figure 2). The GVR resistivity and NeoScope-induced resistivity of the hydrate layer (1425–1442 m, 1445–1450 m, 1455–1465 m, and 1472–1510 m) increased significantly. In addition, the deep, middle, and shallow button images of the GVR showed high-brightness features, and the acoustic velocity became significantly faster.

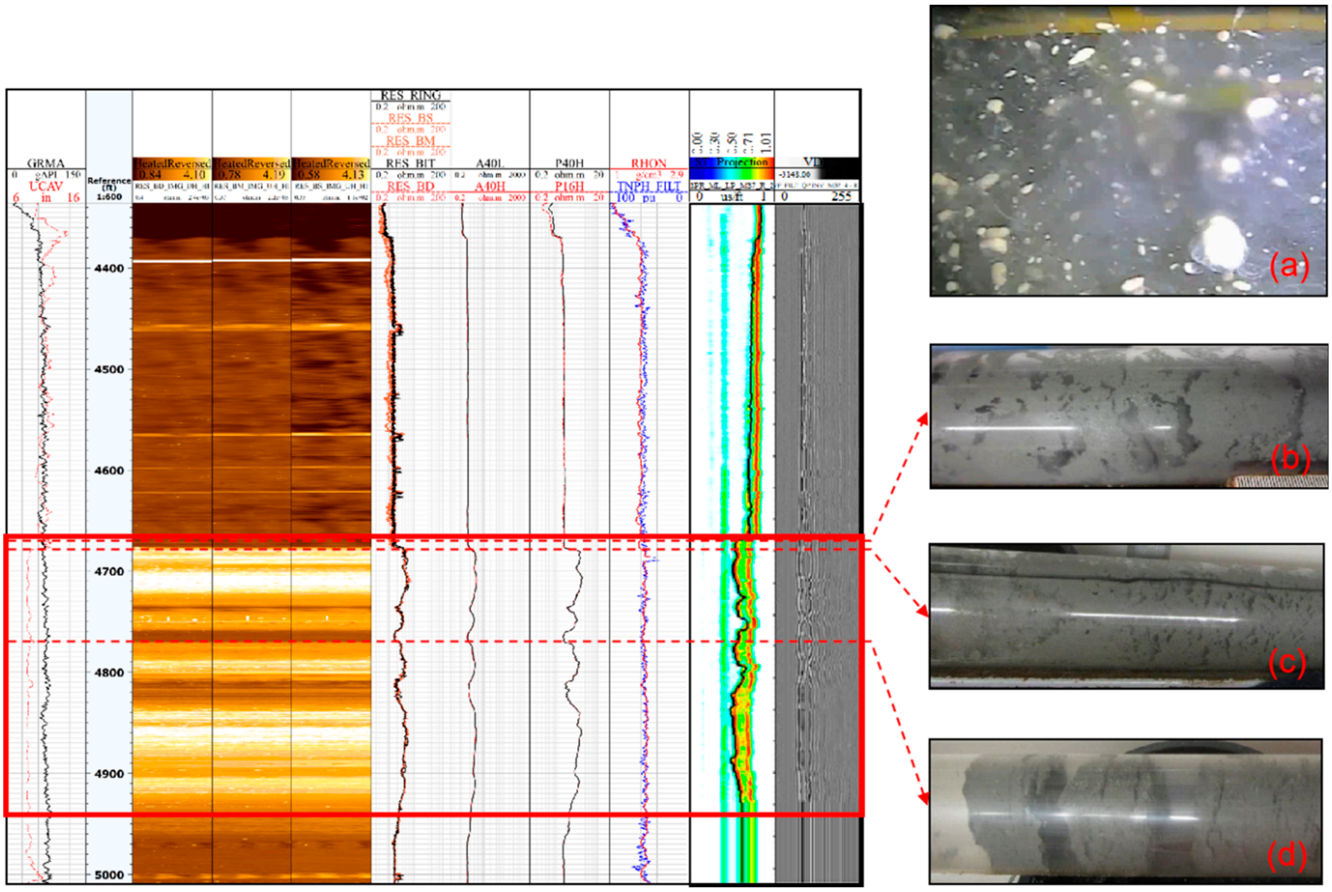

Figure 2. The LWD data and core samples at pilot Well W1: (**a**) the massive hydrate recorded by the seabed camera during the drilling process, where the gas from the hydrate decomposition caused by drilling escapes to the seabed to form hydrates again; (**b**–**d**) partial cores taken from the hydrate layer of well W1B at 1425.95~1426.95 m and 1429.95~1430.95 m, and from well W1C at 1458.45~1460.95 m, respectively. Due to the decomposition of hydrates, the cores are expanded, and the infrared thermal imaging of low-temperature phenomena is evident.

3.2. Methods

According to our discussion in the previous section, in order to evaluate the effects of applying three typical saturation evaluation methods with different principles in the unconsolidated fine-grained sediments, we first introduce the basic principles and petrophysical models of the density NMR logging method, the sigma logging formula, and the Archie formula; then, an innovative method for the calculation of resistance and wave velocity is introduced.

3.2.1. Density NMR Logging Method

Nuclear magnetic resonance (NMR) logging is sensitive to hydrogen in liquids, and the measured NMR amplitude can accurately reflect the porosity of the reservoir [40]. However, the relaxation time of hydrogen atoms in gas hydrates is very short, so the NMR logging tool cannot directly detect hydrate saturation, and it considers hydrates as part of a skeleton. Porosity measured by NMR logging reflects the pore space occupied by water, but not the pore space occupied by gas hydrates. This value is much smaller than the true porosity. While the density log obtains comprehensive information on hydrates and fluids, the difference between density porosity and NMR porosity is the hydrate content (Figure 3).

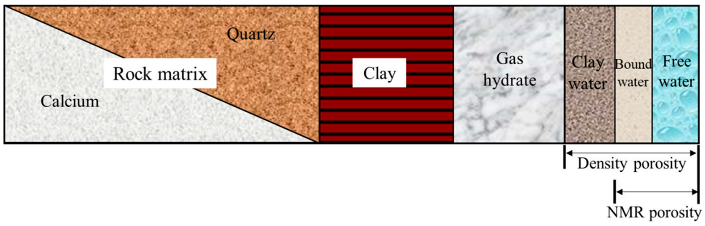

Figure 3. Model of bulk-volume rock of gas-hydrate-bearing sediment reservoirs.

Using this characteristic, we can determine the hydrate saturation by combining the porosity obtained from density logging and NMR logging. The calculation formula is as follows:

$$S_h = (\phi - \phi_{NMR})/\phi \tag{1}$$

where S_h is the hydrate saturation, while ϕ and ϕ_{NMR} are the density porosity and nuclear magnetic porosity, respectively.

3.2.2. Sigma Logging Formula

The probability that a nucleus captures thermal neutrons is called the microscopic capture cross-section of the nucleus. The sum of the microscopic capture cross-sections of all nuclei in a medium of 1 cm^3 is called the macroscopic capture cross-section, denoted by sigma (Σ). Thermal neutrons are absorbed by atomic nuclei in the strata and can release trapped gamma rays. The sigma of the hydrate reservoir can be determined by analyzing the decay curve of the trapped gamma ray count rate over time. The faster the trapped gamma ray count rate decays over time, the higher the sigma value. The formula for calculating sigma is as follows:

$$\Sigma = V_{ma}\Sigma_{ma} + \phi(1 - S_h)\Sigma_w + \phi S_h \Sigma_h \tag{2}$$

By transforming Equation (2), the formula for calculating hydrate saturation by sigma can be obtained:

$$S_h = \frac{(\Sigma_{ma} - \Sigma) + \phi(\Sigma_w - \Sigma_{ma})}{\phi(\Sigma_w - \Sigma_h)} \tag{3}$$

where Σ and ϕ are known quantities, and the values of Σ_{ma}, Σ_w, and Σ_h must also be known if the hydrate saturation is to be obtained. The Σ values range from 4 to 5 c.u. for sandstones, from 5 to 7 c.u. for carbonates, and from 15 to 25 c.u. for clays. The capture cross-section of the rock skeleton is not a fixed value, as it depends on the mineral type and content.

3.2.3. The Archie Formula

The traditional oil and gas method is used to calculate gas saturation via the Archie formula for the logging interpretation of the free gas layer.

$$S_g = 1 - \sqrt[n]{\frac{abR_w}{\phi^m R_t}} \tag{4}$$

where R_w is the formation water's resistivity ($\Omega\cdot$m), m is the cementation index of the formation, a and b are rock-related coefficients, R_t is the formation's resistivity ($\Omega\cdot$m), n is the saturation index, and S_g is the gas saturation.

The values of formation parameters a, b, m, and n are related to lithology and have regional characteristics, which can be obtained through core experiments. Generally speaking, a is 0.6–1.5, m is between 1.5 and 3, b is close to 1, and n ranges from 1.5 to 2.2. However, the target strata in the study area are unconsolidated fine-grained sediments, and the formation parameters cannot be obtained from the core via conventional experiments. The key to research is to estimate the formation parameters a, b, m, and n by combining reservoir characteristics and logging response characteristics.

Therefore, in the context of fewer systematic petrophysical reservoir experiments with logging evaluation as our ultimate goal, we needed to study the values of the electrical parameters of rocks in gas hydrate reservoirs using resistivity logging data. Confronted with the difficulty of obtaining the electrical parameters of the rocks through experiments, we used the logged resistivity values of the water-sediment layer without gas hydrate as the benchmark to calculate the electrical parameters [26]. We selected porosity and resistivity data corresponding to some core data points with gas hydrate saturation of less than 10%, as determined by coring experiments, as the core data for analysis. Since the target strata are located in the seabed and are loose and unconsolidated, they can be considered non-hydrate and gas strata. The pore space is completely saturated with water, so the measured resistivity of the completely water-saturated strata is R_0.

The formation factor F in the Archie formula is expressed as follows:

$$F = \frac{R_0}{R_w} = \frac{a}{\phi^m} \tag{5}$$

where R_0 is the formation's resistivity when 100% filled with formation water ($\Omega \cdot$m). We assume that the logging resistivity of core data with hydrate saturation less than 10% is R_0, so we only need to obtain R_w, which is the resistivity of the formation water ($\Omega \cdot$m).

According to the data, the degree of mineralization of the formation water in the study area ranges from 32 ppk to 34 ppk, and the calculated resistivity of formation water is between 0.338 and 0.356 $\Omega \cdot$m. Therefore, the average value of 0.34 $\Omega \cdot$m can be taken as R_w. In this way, the formation factor F can be obtained, and the method of finding the porosity ϕ can be known. Furthermore, the values of a and m can be determined by drawing the F–ϕ curve in the double-logarithmic coordinates.

The increasing resistivity coefficient I in the Archie formula is expressed as follows:

$$I = \frac{R_t}{R_0} = \frac{b}{S_w^n} = \frac{b}{(1 - S_o)^n} \tag{6}$$

where R_t is the resistivity of the oil-bearing formation ($\Omega \cdot$m), while S_w and S_o are the water saturation and oil saturation of the formation, respectively. Since the gas saturation cannot be measured, the electrical variation of the strata with different hydrate saturation was studied, so Equation (6) was changed into Equation (7):

$$I = \frac{R_t}{R_0} = \frac{b}{S_w^n} = \frac{b}{(1 - S_h)^n} \tag{7}$$

where R_t is the resistivity of the hydrate-containing formation ($\Omega \cdot$m), while S_h is the hydrate saturation in the formation. Using the well data, the I–S_w curve in double-logarithmic coordinates was drawn, and the values of the parameters b and n were determined through data-fitting analysis. When the formation parameters a, b, m, and n are obtained, the water saturation can be calculated using the Archie formula. However, it should be noted that only the rocks' electrical data are reliable. Based on the theory, the estimation results obtained from the hydrate test data using the formation characteristics and logging response characteristics have certain reference values. However, the accuracy of the parameters needs to be verified.

3.2.4. Resistivity DT Logging Method

The resistivity and wave velocity are most obviously affected by hydrates in well-logging data. The relatively high resistivity and acoustic velocity are typical logging response characteristics of hydrate reservoirs. Therefore, a two-parameter model of resistivity and the acoustic time difference was established to calculate hydrate saturation.

$$S_h = a\lg\left(\frac{RT}{RT_{\text{baseline}}}\right) + b\lg\left(\frac{AC_{\text{baseline}}}{AC}\right) \tag{8}$$

where RT is the deep resistivity (Ω·m), RT_{baseline} is the deep resistivity baseline (Ω·m), AC is the acoustic time difference (μs/m), AC_{baseline} is the baseline of the acoustic time difference (μs/m), and a and b are the coefficients.

Making $\lg R = \lg(\frac{RT}{RT_{\text{baseline}}})$, $\lg\Delta t = \lg(\frac{AC_{\text{baseline}}}{AC})$, by dividing both sides of Equation (8) by $\lg R$, we can get

$$S_h/\lg R = a + b(\lg\Delta t/\lg R) \tag{9}$$

Obviously, Formula (9) is in the form of y = A + Bx, from which the values of the coefficients A and B can be fitted by linear regression. Then, the saturation calculation formula can be determined.

4. Results

4.1. Density NMR Logging Method

The hydrate saturation obtained via the saturation calculation method given in Section 3.2.1 and the density NMR logging method is independent of the reservoir model and parameters; it is only related to the accuracy of NMR and density logging. Figure 4 shows the processing results of the saturation model of density NMR logging. The first channel is the lithology, including the natural gamma (GRMA) and caliper curves (UCAV); the second is the resistivity, including two resistivity curves; the third is the depth channel, indicating the well depth; the fourth is the porosity, including the density (RHON), neutron (TNPH_FILT), and acoustic wave (DTCO) curves; and the fifth is the NMR T2 spectrum; the sixth is the porosity, which includes the total porosity (PHIT_QEPP, red line) and NMR porosity (MRP, black line). Finally, there are curve channels of gas hydrate saturation. The SH and SH_NMR (green filling) are those determined from the core density NMR logging method. From the 4510–4600-feet section of Well W3 in Figure 4, it can be seen that the average hydrate saturation content of the core is 2.7%. Combined with the low resistivity and other logging curve response values, this section can be considered to be a non-hydrate reservoir. As demonstrated above, the porosity obtained by NMR logging in a non-hydrate layer is the total porosity, which matches well with the NMR porosity. The calculated hydrate saturation values are generally consistent with the core saturation data, indicating that the density NMR method for saturation calculation is theoretically feasible. However, the scarcity of NMR logs in the shallow strata, the low data acquisition rate, and the reliability of NMR porosity limit its application in the evaluation of saturation.

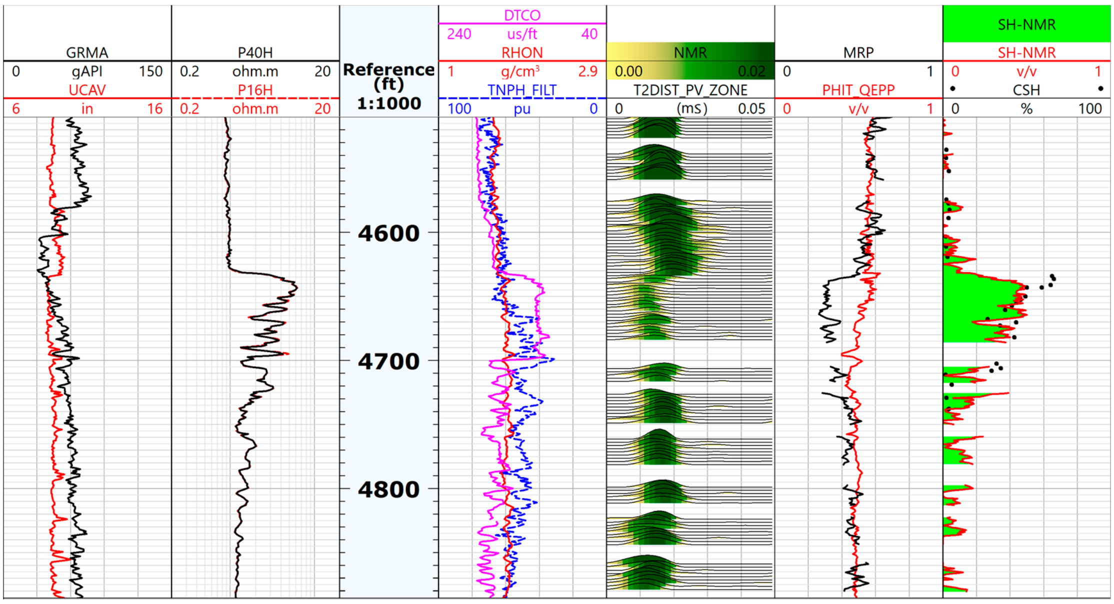

Figure 4. Comparison of the processing results of NMR logging saturation models with core data.

4.2. Sigma Logging Formula

The key to calculating saturation using the sigma logging formula is accurately determining Σ_w, Σ_h, and Σ_{ma}. The capture cross-section of formation water is related to temperature and salinity and increases with the salinity. By comparing multiple wells in the study area, we found that the sigma curve had a stable value within the range of 0~7 m from the seabed. According to the sequence of LWD tool strings, the logging tool near the bottom was GeoVision, followed by NeoScope, TeleScope, SonicScope, and ProVision. Therefore, it can be considered that the initial measurement value of the capture cross-section Σ should be the Σ of seawater. Because the target layer is shallow, it can be derived that the formation water is consistent with seawater. It can be seen from the multiple wells in the study area that Σ_w is ~43–45 c.u. Figure 5 provides an example of the formation water layer of Well W3. The porosity in the 4586–4627-feet interval is 0.6, with a measured sigma value of 28 c.u. The rock skeleton is mainly composed of sandstone and illite rocks, with a value of 7 c.u. Substituting the parameters into Equation (2), Σ_w can be calculated as 44 c.u.

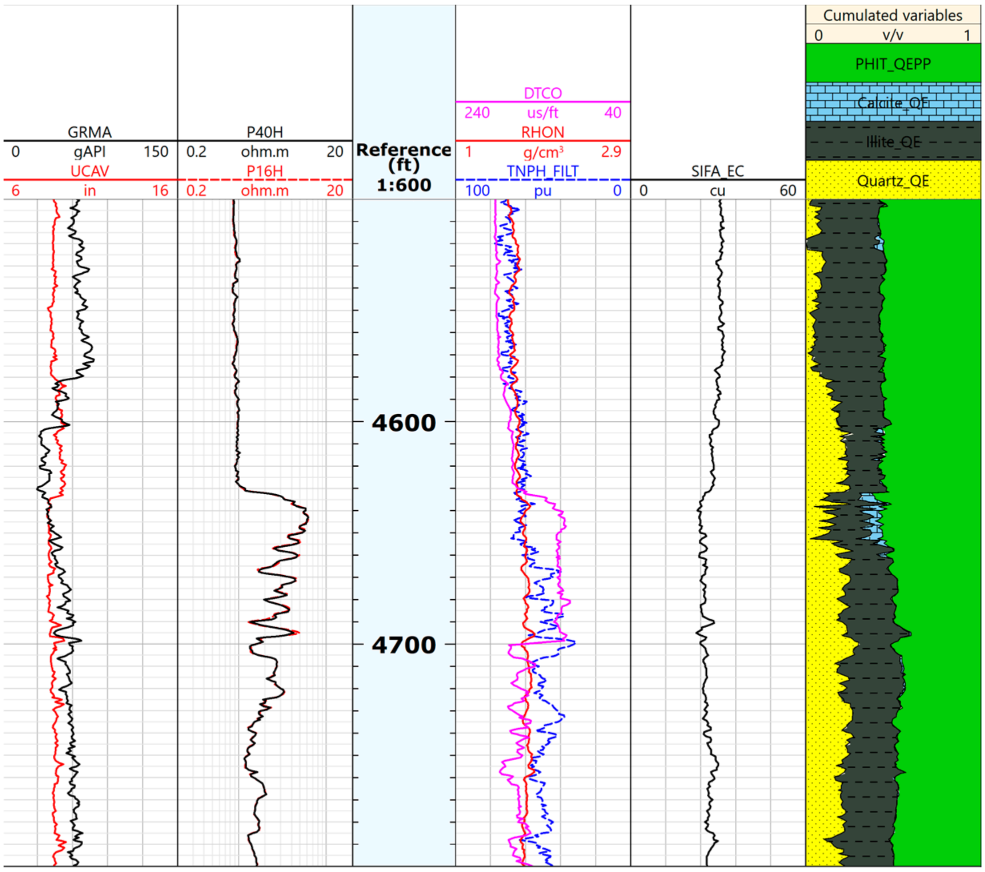

Figure 5. Well W3's logging curve and measured sigma value.

Taking the hydrate formations of Well W1 and Well W2 as examples, the capture cross-section of the gas hydrates was calculated by using Formula (3). Figure 6 shows the hydrate saturation results calculated using sigma for the two wells. The first channel is the lithology, including the natural gamma (GRMA) and caliper curves (UCAV); the second is the resistivity, including two resistivity curves; the third is the depth channel, indicating the depth of the well; the fourth is the porosity, which includes the density (RHON), neutron (TNPH_FILT), and acoustic wave (DTCO) curves; and the fifth is the $\sum$ (SIFA_EC); the sixth is the lithological profile. Finally, there are curve channels of gas hydrate saturation. The CSH and SH (green filling) are those determined from the core sigma logging formula.

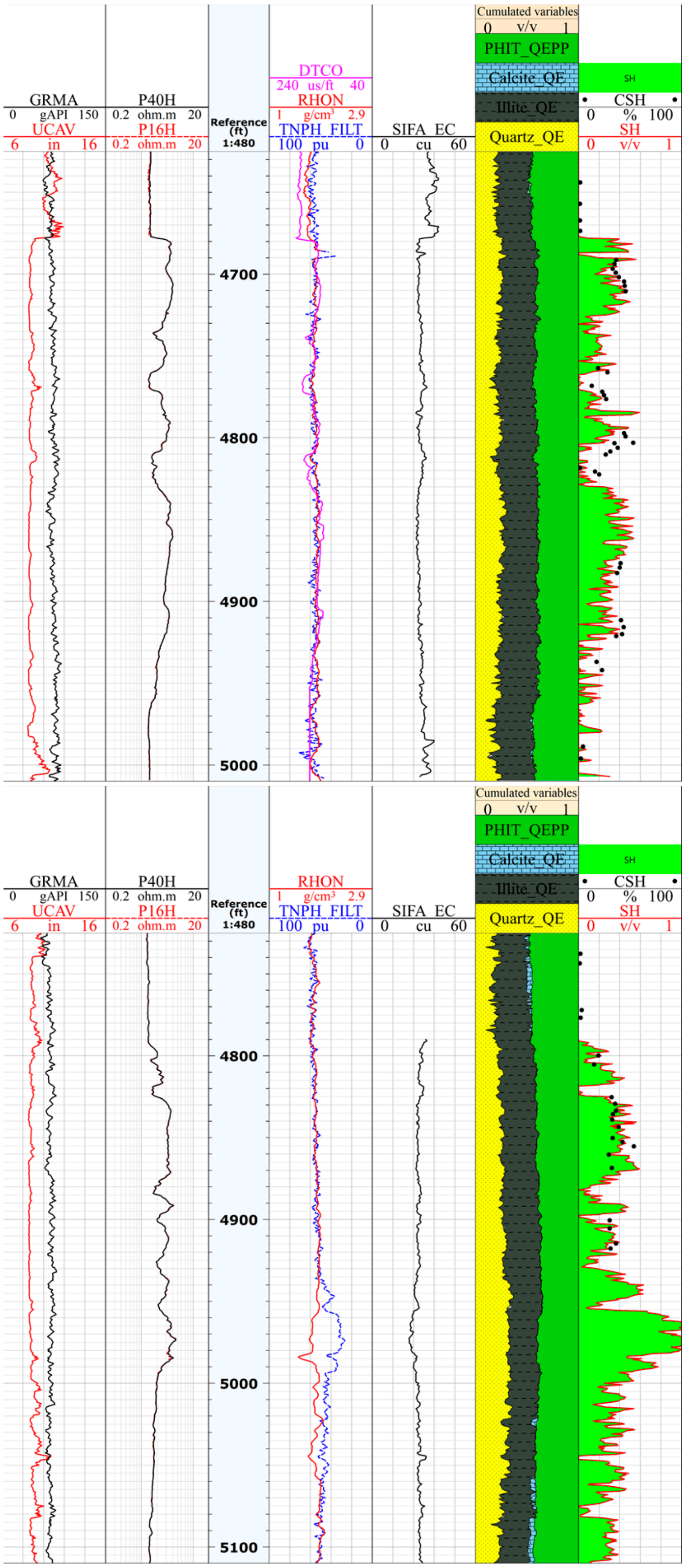

Figure 6. Sigma logging saturation model and core data in Wells W1 and W2.

The calculation of hydrate saturation is greatly affected by lithology, and the clay contents of Wells W1, W2, and W3 gradually decrease. In the calculation, the $\sum_{ma}$ values were 19 c.u., 15 c.u., and 7 c.u. In order to match the core saturation, the $\sum$ value of natural gas was ~12 c.u., and the measured $\sum$ decreased with the increase in gas content. There was a gas layer in Well W2, and the hydrate saturation calculated according to the formula was relatively large.

4.3. The Archie Formula

The Archie formula estimates the electrical parameters of rocks in gas hydrate reservoirs using resistivity logging data. We selected porosity and resistivity data corresponding to some core data points with gas hydrate saturation of less than 10%, as determined by coring experiments in four wells, as the core data for analysis. Since the target strata are located in the seabed and are loose and unconsolidated, they can be considered non-hydrate and gas strata. The pore space is completely saturated with water, so the measured resistivity is the resistivity R_0 of completely water-saturated strata. Figure 7a shows the F–ϕ curve in double-logarithmic coordinates drawn using the data of Wells W1, W2, W3, and W4. There are 41 sample points for Well W1, 303 for Well W2, 347 for Well W3, and 379 for Well W4. The data fitting results show that the F–ϕ relationship is $F = 1.3563 \times \phi^{-1.641}$, which is essentially a straight line consistent with the theoretical relationship, so $a = 1.3563$ and $m = 1.641$ can be obtained. Figure 7b shows the I–S_w relationship curve in double-logarithmic coordinates drawn using the data of Wells W1, W2, W3, and W4. The data-fitting result shows that the I–S_w relationship is $I = 0.997 \times S_w{}^{-1.7}$, which is essentially a straight line consistent with the theoretical relationship, so $b = 0.997$ and $n = 1.7$ can be obtained. When the formation parameters a, b, m, and n are obtained, the gas saturation can be calculated using the Archie formula.

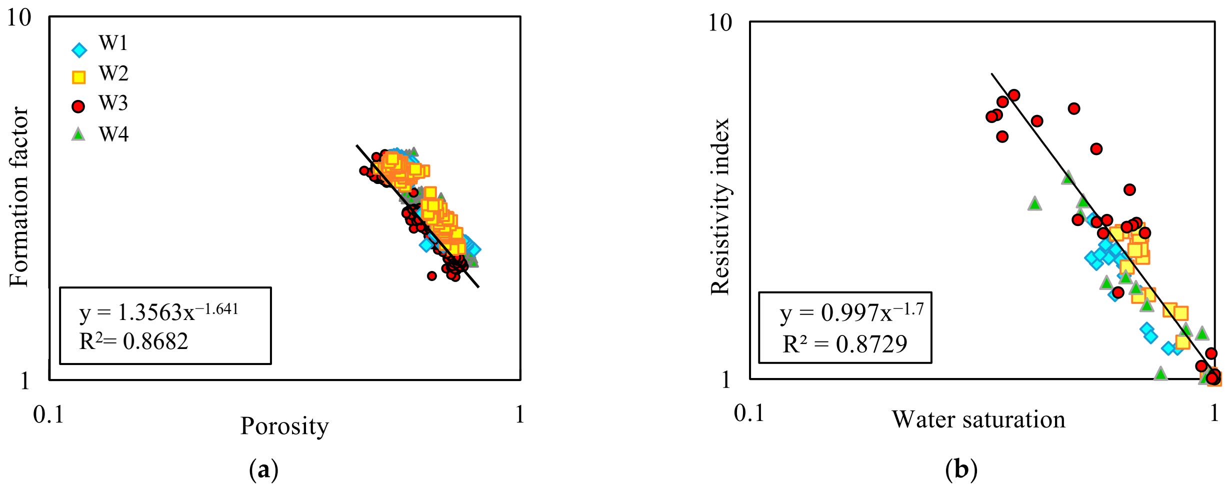

Figure 7. Rock–electricity relationships in the study area. (**a**) Relationship between formation factors and porosity. (**b**) Relation between resistivity index and water saturation.

The saturation was calculated using the Archie formula and the values of the parameters a, b, m, and n. In order to better evaluate the saturation results, we applied the above methods to the four wells in the study area, taking wells W1, W2, and W4 as examples (Figure 8). In Figure 8, the first channel is the lithology, including the natural gamma (GRMA) and caliper curves (UCAV); the second is the resistivity, including two resistivity curves; the third is the depth channel, indicating the depth of the well; the fourth is the porosity, which includes the density (RHON), neutron (TNPH_FILT), and acoustic wave (DTCO) curves; and the fifth is the lithological profile. Finally, there are curve channels of gas hydrate saturation. The CSH and SH are those determined from the core Archie formula. From W1, W2, and W4, the calculated hydrate saturation values are generally consistent with the core saturation data, indicating that the Archie formula is theoretically feasible for saturation calculation—especially in the high-quality reservoir section (4680–4950 feet in W1). Based on the calculation results of the Archie formula in the three wells, it is found that the formation with high evaluation accuracy has a relatively high sandstone content, which is a relatively coarse-grained high gas hydrate reservoir. Compared with conventional reservoirs, it is challenging to carry out electrical experiments on rocks in unconsolidated sediments. From the results, clay content, particle size, and pore structure may all affect the value of *a*, *b*, *m*, *n*, and the specific laws of rock electrical parameters need more in-depth analysis based on rock electrical experiments.

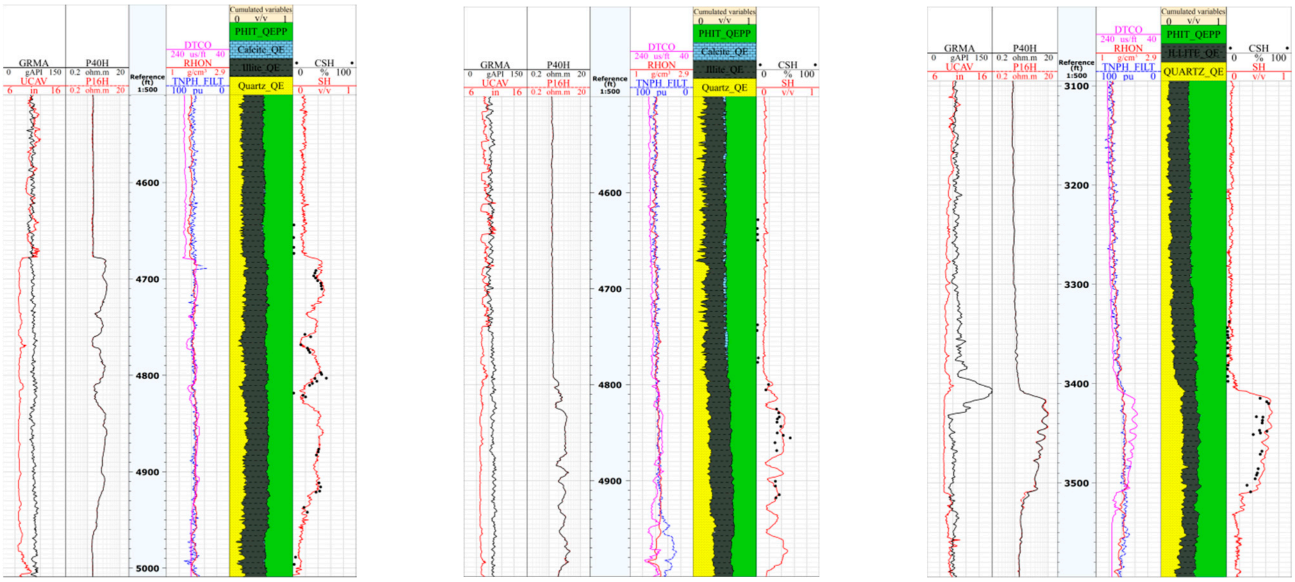

Figure 8. Archie saturation model and core data in Wells W1, W2, and W4.

4.4. Resistivity DT Logging Method

The resistivity DT logging method is a new method to evaluate hydrate saturation. Gas hydrate saturation must correspond to relatively high resistivity and acoustic velocity. The saturation experimental data of Wells W1, W2, and W4 were selected for fitting. In addition, Wells T1 and T2 outside the study area were selected to verify the applicability of the method. The LWD P40H curve was selected for the deep resistivity, and the DTCO curve was selected for the acoustic time difference. The fitting results are shown in Table 1 and Figure 9.

Table 1. Coefficient fitting of the resistivity–acoustic time difference formula.

WELL	Coefficient		Coefficient of Determination	Correlation Coefficient
	a	*b*	R^2	*R*
W1	0.1989	3.0211	0.9110	0.9545
W2	0.3146	2.8776	0.9638	0.9817
W4	0.1778	2.3017	0.9061	0.9519
T1	0.2077	2.3230	0.9295	0.9641
T2	0.1356	2.5172	0.8978	0.9475
Arithmetic	0.2069	2.6081	0.9216	0.9599
Standard deviation	0.0044	0.1067	/	
Variance	0.0663	0.3266		

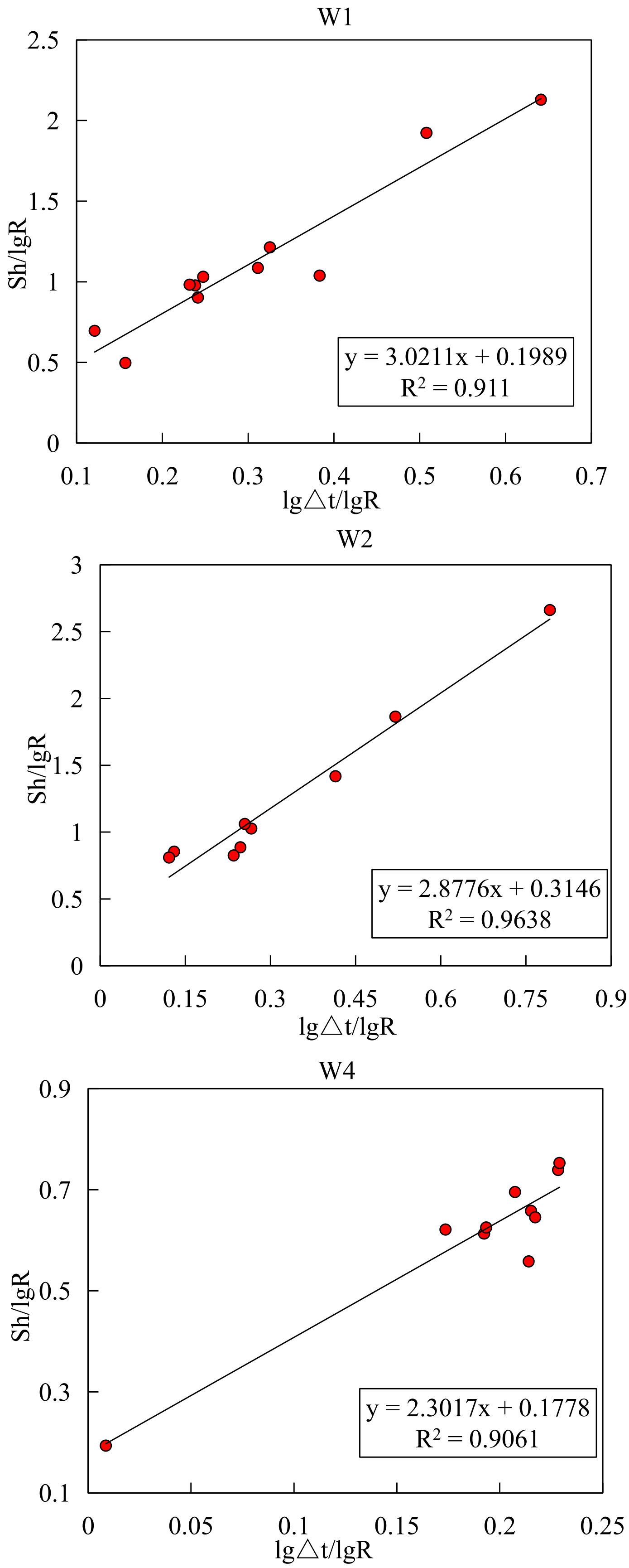

Figure 9. *Cont.*

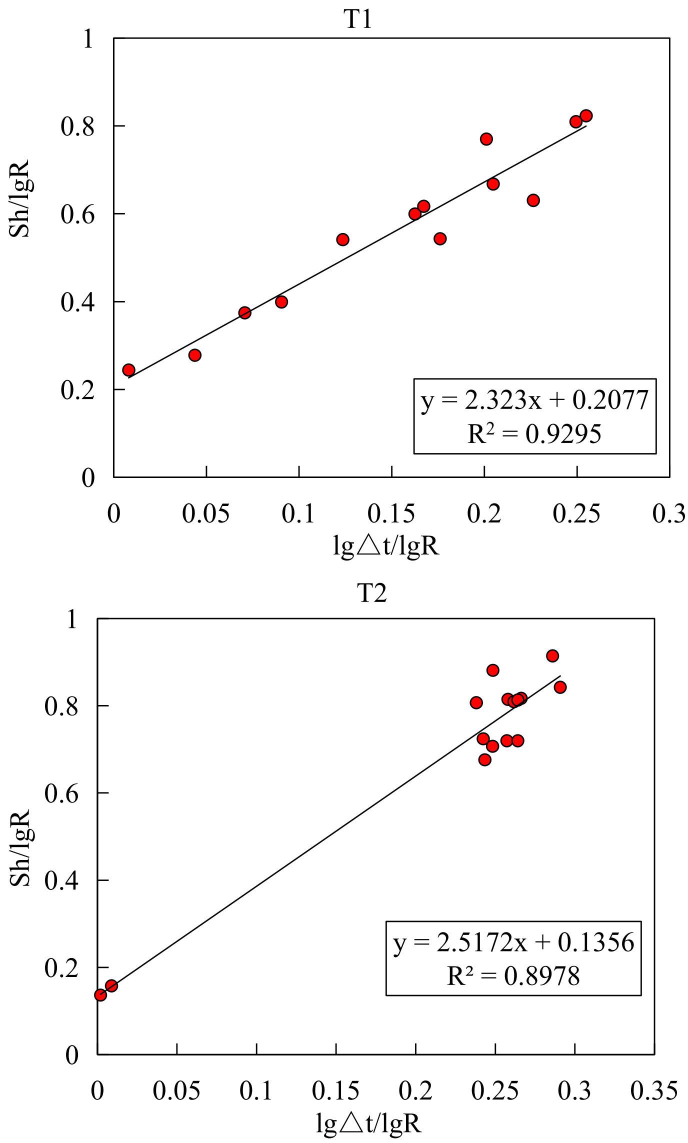

Figure 9. Coefficient fitting diagram of resistivity–acoustic time difference formula.

The fitting coefficient values can be obtained from Table 1, and each data group has a strong correlation. For example, the values of coefficients A and B obtained by calculating the arithmetic average are 0.2069 and 2.6081, respectively. Thus, Equation (8) can be expressed as follows:

$$S_h = 0.2069\lg(\frac{P40H}{P40H_{\text{baseline}}}) + 2.6081\lg(\frac{DTCO_{\text{baseline}}}{DTCO}) \tag{10}$$

The above equation was used to recalculate all wells with experimental saturation data to verify the adaptability of the formula. The calculation results for W1, W2, W3, and W4 are shown in Figure 10 according to the saturation model of the resistivity DT logging method. The first channel is the lithology, including the natural gamma (GRMA) and caliper curves (UCAV); the second is the resistivity, including two resistivity curves; the third is the depth channel, indicating the depth of the well; and the fourth is the porosity, including the density (RHON), neutron (TNPH_FILT), and acoustic wave (DTCO) curves. Finally, there are curve channels of gas hydrate saturation. The CSH and SH-RT-DT (green filling) are those determined from the core resistivity DT logging method. This method has high accuracy in both reservoir and non-reservoir and can better reflect the saturation characteristics of high-quality reservoirs.

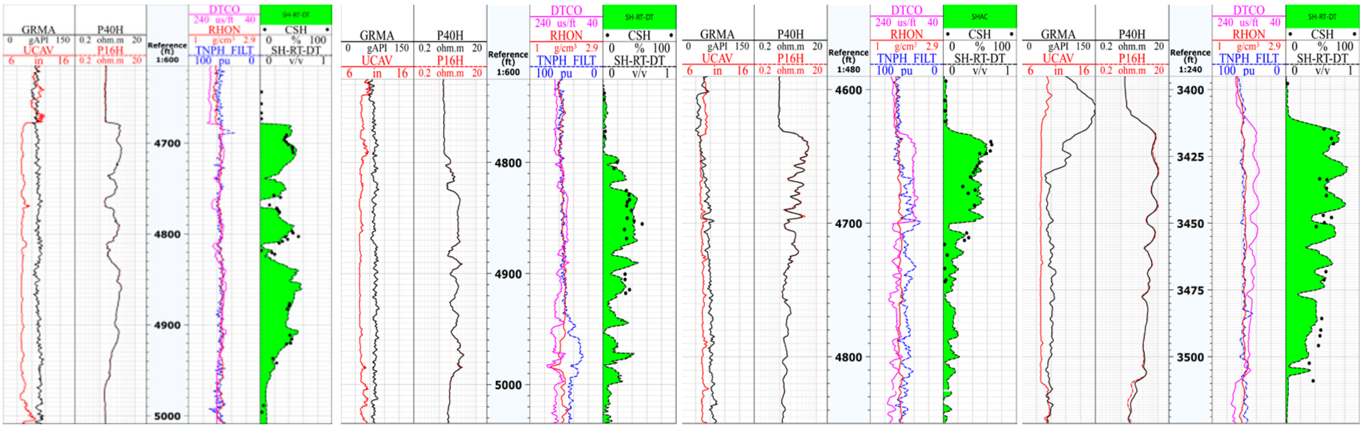

Figure 10. Gas hydrate saturation by using resistivity DT logging in W1, W2, W3, and W4.

5. Discussion

5.1. Practicability of Each Well-Logging Method

A high-precision model was used to calculate the gas hydrate saturation in the sediments. In order to fully verify the calculation accuracy and applicability of each model, the above four methods were applied to Well W03; Figure 11 shows the calculation results. The first channel in Figure 11 is the lithology, including the natural gamma (GRMA) and caliper curves (UCAV); the second is the resistivity, including two resistivity curves; the third is the depth channel, indicating the depth of the well; the fourth is the porosity, which includes the density (RHON), neutron (TNPH_FILT), and acoustic wave (DTCO) curves; the fifth is the NMR T2 spectrum; the sixth is the lithological profile; the seventh is the calculation results of the resistivity DT logging method model (SH-RT-DT (green filling)); the eighth is the calculation results of the density NMR logging method (SH-NMR (green filling)); and the ninth is the sigma calculation results (SH-Σ (green filling)). Finally, there are the Archie formula calculation results (SH-ARCHIE (green filling)). The results from Figure 11 confirm that all four methods can effectively reflect the overall changing trend of reservoir saturation. Among them, the hydrate content above 4628 feet is low, and the saturation between 4628 and 4700 feet is high, indicating a good hydrate reservoir. The density NMR logging method's calculation results show good performance in some small layers, such as the 4669.38–4683.3-feet section of Well W3. However, for the density NMR logging, the following problems remain: (1) There are few nuclear magnetic logs in the region, and the data acquisition rate is low. (2) In the well section where nuclear magnetic logging is conducted, there are some missing layers due to measurement problems (such as at 4685–4703 feet in W3), seriously affecting the application of this method. (3) The reliability of NMR porosity needs to be verified. When the sediment contains a large amount of bound water related to clay minerals, T2 will increase, and the NMR porosity will be underestimated, affecting the accuracy of the estimated hydrate saturation (such as at 4629–4660 feet in W3). (4) Due to the changes in lithology and mineral composition in the study area, inaccurate matrix density leads to errors in the calculation of density porosity.

As for the sigma logging formula, through the analysis of the adaptability of the sigma saturation model of the capture section, the following understandings were obtained: (1) According to the element mineral measurement results using NeoScope, there may be significant errors in the measurement of sigma. (2) This method applies only to relatively pure sandstone or carbonate rock; for strata with high clay content, it is difficult to determine the rock skeleton, and the calculation is unreliable. (3) The method is suitable for high-salinity strata. (4) For gas-bearing formations, Σ decreases, and the calculated hydrate saturation is too large. In conclusion, the errors in the calculation of hydrate saturation using sigma are large, due to measurement error and uncertainties in the skeleton values. In addition, one more issue needs to be clarified: the sigma plate produced by Schlumberger allows us to obtain sigma values of formation water at different temperatures, pressures, and mineralization levels. The salinity of formation water in the study area is ~33 ppk, the temperature of hydrate formation is 12–14 °C, and the pressure is ~13 Mpa. Therefore, the sigma value of formation water obtained by using the plate was ~33 c.u., which is different from the value calculated above. The reason for this difference is still uncertain. The inaccurate value of Σw may also be the reason for the low accuracy of the sigma logging formula.

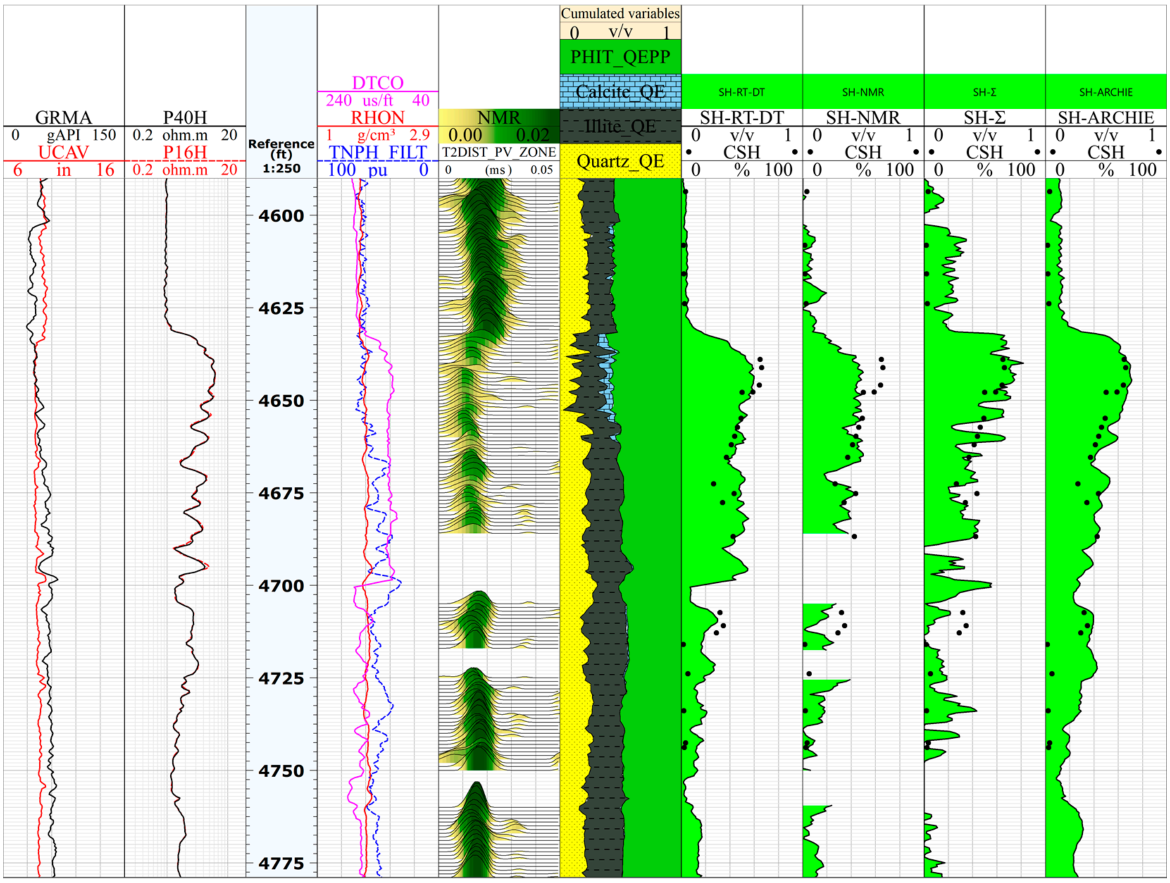

Figure 11. Comparison of various logging saturation calculation methods for Well W3.

Nevertheless, estimating natural gas hydrate saturation using the Archie formula is different from the calculation of conventional oil–gas characteristics in diagenetic formations. It is difficult to accurately determine the electrical parameters of the rocks using this formula, which makes it difficult to ensure the calculations' accuracy in unconsolidated sediments. After accurately obtaining the electrical parameters of the rocks, the accuracy of the saturation calculation using the Archie formula is high and can be applied to high-quality reservoir sections. For example, at 4632–4700 feet, the calculated hydrate saturation values are generally consistent with the core saturation data, indicating that the Archie formula is theoretically feasible for calculating saturation in the high-quality reservoir section. However, due to the dissociation of hydrates during drilling, the salinity of the pore fluid will decrease, increasing the resistivity of the logging data. In addition, the formation being filled with natural gas will lead to an increase in its electrical properties [41]; therefore, it cannot be distinguished from hydrates. The hydrate saturation calculated according to the resistivity logs may represent the maximum estimate of hydrate saturation.

As shown in Figures 11 and 12, we compared various logging saturation calculation methods with the results of core saturation, which were derived from the resistivity DT logging method, density NMR logging method, sigma logging formula, and the Archie formula predictions. The core saturation data used in this paper were derived from the field analysis and test results of constant-pressure coring. During the drilling process, according to the logging results, while drilling the pilot wells, core drilling was carried out in the area within 20 m of the pilot wells for the gas hydrate layer. The testing process was as follows: The constant-pressure core was first sent to the relevant laboratory, and the core gamma, acoustic, and density tests were carried out to calculate the core porosity. After that, pressure relief and degassing equipment were used to slowly release the pressure and collect the gas released by the decomposition of the natural gas hydrates, and the gas hydrate saturation of the core was calculated from the gas volume and the concentration changes after chlorine ion desalination caused by the decomposition of the natural gas hydrates. To better analyze the effects of the model's application, we divided the verification well into three sections according to the reservoir quality; the first section was 4540–4627 m, the second section was 4627–4702 m, and the third section was 4702–4775 m. In the first section, the saturation calculated by the resistivity DT logging method coincided well with the core saturation, with a relative error of 4.35%, whereas that of the other three typical method calculation results was too large. As for the second section, the overall average relative error calculated by the resistivity DT logging method was 0.91%, while the best of the other three methods was 1.03%. The errors in the third section were slightly higher; intervals may have been caused by the increase in acoustic time difference, high saturation of the gas reservoir, logging curve quality problems, resolution factors, and experimental errors. However, the mean relative error of the three reservoirs using the resistivity DT logging method was 5.87%; in general, this method improves the calculation accuracy of hydrate saturation and reduces the influence of natural gas in the formation. Evidently, for the resistivity DT logging method, both the low- and high-saturation intervals have good calculation results. On the other hand, the calculation accuracy of the density NMR logging method and the sigma logging formula is low, while the Archie formula generally predicts higher than core data.

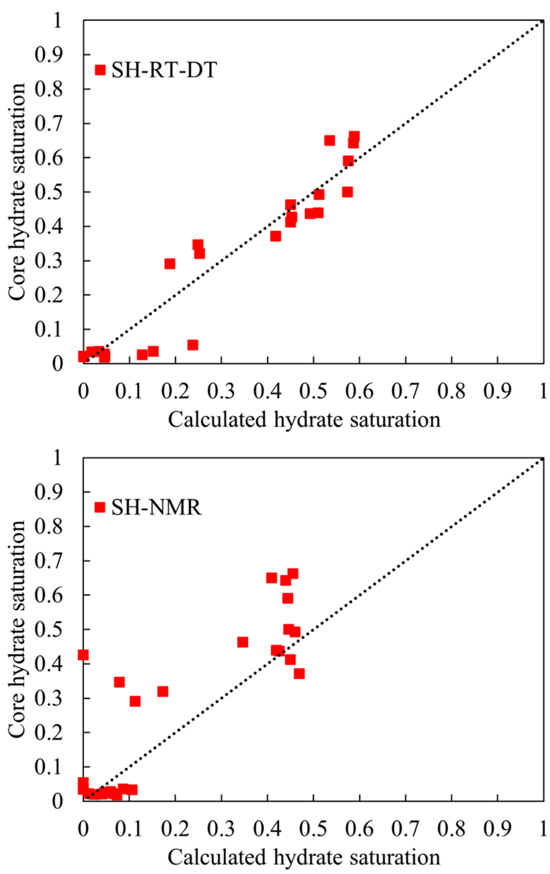

Figure 12. *Cont.*

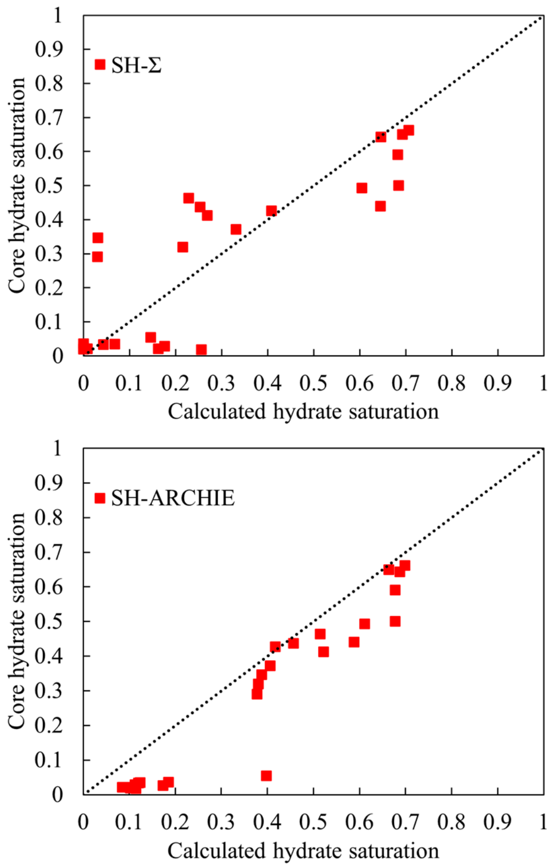

Figure 12. Comparison of various methods for the calculation of logging saturation with core saturation.

5.2. Rapid Discrimination of Gas Hydrate Saturation in a Resistivity–Acoustic Time Difference Cross Chart

Quick discrimination of gas hydrate saturation is necessary during the drilling of wells. Based on the determination of the saturation calculation method, through the analysis of Formula (10), we can derive the following:

$$P40H = 10^{4.83Sh} \cdot P40H_{\text{baseline}} \cdot \left(\frac{DTCO}{DTCO_{\text{baseline}}}\right)^{12.6} \tag{11}$$

As long as appropriate base values of resistivity and acoustic time differences are selected, a set of resistivity–acoustic time difference cross charts (Figure 13) related to hydrate saturation can be established by using the above formula to achieve rapid discrimination of hydrate saturation during logging construction.

In order to verify the effects of the resistivity–acoustic time difference cross chart, we used Well T1 for testing. Well T1 is approximately 2.6, 1, 4.4, and 10.8 km away from Wells W1, W2, W3, and W4, respectively. The LWD data were acquired during the GMGS4 gas hydrate expedition cruise in 2017. The above four drilling sites all include pilot holes and core holes. The LWD pilot hole mainly provides resistivity, acoustic wave, density, neutron, and gamma-ray logging data while drilling, and it monitors resistivity, acoustic wave, and gamma-ray logging in real-time. The core hole mainly provides core data, including core saturation data. The logging curves of the acoustic wave (DTCO) and resistivity (P40H) for Well T1 are shown in Figure 14. From the figure, we can see that Well T1 can be divided into three sections according to the quality of the reservoir. The saturation content of T1-1 (1400–1432 m) and T1-3 (1459–1480 m) is low, where the core saturation of T1-1 is 6.75% on average, and the average core saturation of T1-3 is 6.56%. We put the logging curves corresponding to the two sections of cores into the resistivity–acoustic time difference cross chart to judge the hydrate layer quickly. It can be seen that the data typically fall in the area with a saturation of less than 10%. These results are consistent with the core results, which can quickly identify the low-saturation layer. As for T1-2, the saturation content is high, with a maximum saturation of 61.33806% and an average of 33.13%. We put the logging curves of T1-2 into the resistivity–acoustic time difference cross chart. It can be seen that the data results cover the 0.1–0.6 area, with the highest saturation above 0.6—especially at 1435.5–1442 m, where the saturation is higher than 50%. Therefore, the resistivity–acoustic time difference cross chart can rapidly determine gas hydrates' saturation during drilling.

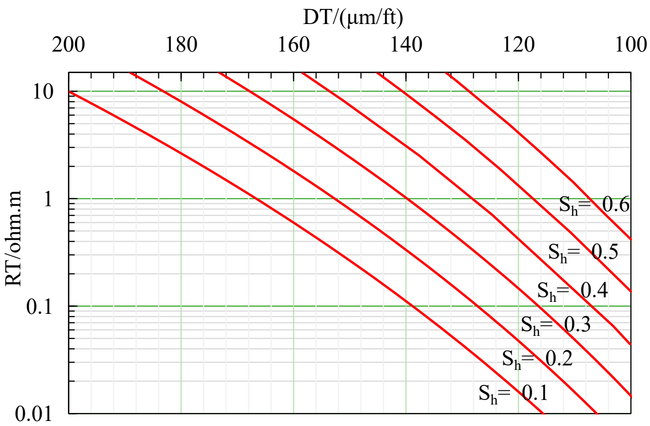

Figure 13. Resistivity–acoustic time difference cross chart.

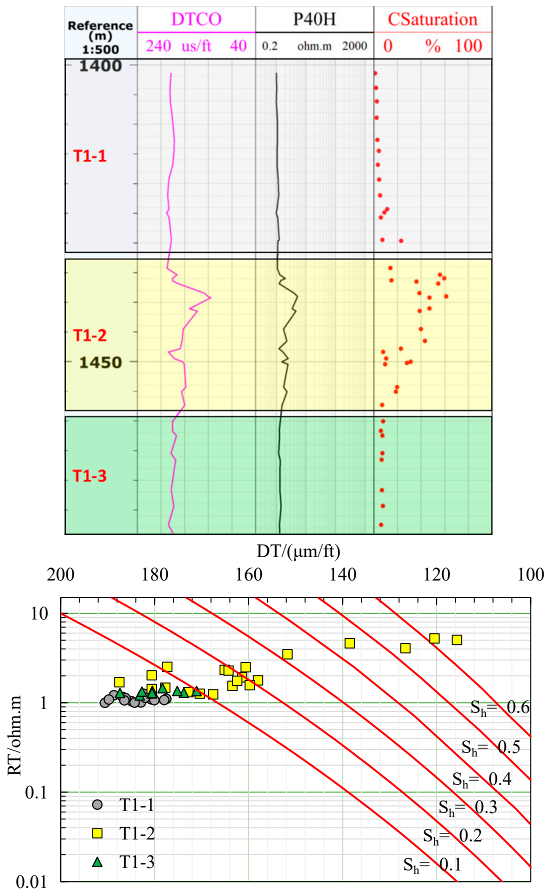

Figure 14. Well T1's logging curves and quick recognition results from the resistivity–acoustic time difference cross chart of the key layer.

6. Conclusions

Based on the LWD logging data for four wells during GMGS3 and GMGS4, the gas hydrate saturation in the northern South China Sea was calculated using three typical methods for the evaluation of saturation with different principles in the unconsolidated fine-grained sediments: density NMR logging, sigma logging, and the Archie formula. The verification results confirmed that all three methods could effectively reflect the overall change in the trend of reservoir saturation. However, each method has applicable conditions and limitations. For the density NMR logging method, the following problems remain: Due to the measurement method, it is difficult to guarantee the quantity and quality of some nuclear magnetic logging, seriously affecting the application of this method. Additionally, the reliability of NMR porosity needs to be verified. When the sediment contains a large amount of bound water related to clay minerals, T2 will increase, and NMR porosity will be underestimated, affecting the accuracy of the estimated hydrate saturation. Furthermore, due to the changes in lithology and mineral composition in the study area, inaccurate matrix density leads to errors in the calculation of density porosity. As for sigma logging, the errors in the calculation of hydrate saturation using sigma are large due to measurement error and uncertainties in the skeleton values. The Archie formula is different from the conventional calculation of oil–gas characteristics in diagenetic formations. It is difficult to accurately determine the electrical parameters of the rocks from the experimental results, making it difficult to ensure the accuracy of calculations in unconsolidated sediments. After accurately obtaining the electrical parameters of the rocks, the saturation calculation accuracy of the Archie formula is high, and it can be applied to high-quality reservoir sections.

An innovative bivariate resistivity DT logging method is proposed to calculate saturation. This algorithm avoids the influence of uncertainty in the electrical parameters of the rocks in the Archie formula, as well as the influence of uncertain lithological capture cross-sections in sigma calculation. The overall relative error of the verification well was 5.87%, representing a dramatic improvement in the calculation accuracy of hydrate saturation.

Author Contributions: Methodology, X.W. and X.W.; Formal analysis, J.L. (Jingan Lu); Investigation, C.W. and R.W.; Resources, J.L. (Jinqiang Liang); Writing—original draft, X.Z.; Writing—review & editing, S.W.; Visualization, B.L.; Supervision, X.W. All authors have read and agreed to the published version of the manuscript.

Funding: This research was funded by the Hainan Provincial Joint Project of Sanya Yazhou Bay Science and Technology City (No. 2021JJLH0017), Hainan Provincial Natural Science Foundation of China (No. 422QN355), Open Foundation of Key Laboratory of Marine Mineral Resources, Ministry of Natural Resources (No. KLMMR-2015-A-15).

Data Availability Statement: Not applicable.

Conflicts of Interest: The authors declare no conflict of interest.

References

1. Kvenvolden, K.A. Gas hydrates-geological perspective and global change. *Rev. Geophys.* **1993**, *31*, 173–187. [CrossRef]
2. Sloan, E.D. *Clathrate Hydrates of Natural Gases*, 2nd ed.; Marcel Dekker Inc.: New York, NY, USA, 1998; 628p.
3. Collett, T.S.; Lee, M.W.; Goldberg, D.S. *Data Report: Nuclear Magnetic Resonance Logging while Drilling, ODP Leg 204*; College Station, Ocean Drilling Program: Texas, TX, USA, 2006; pp. 1–22.
4. Zhang, H.Q.; Yang, S.X.; Wu, N.Y.; Xu, X.; Melanie, H.; Peter, S.; Kelly, R.; Heather, B.; Gary, H.; GMGS-1 Science Team. Successful and surprising results for China's first gas hydrate drilling expedition. In *Fire in the Ice. Methane Hydrate Newsletter*; National Energy Technology Laboratory, US Department of Energy: Pittsburgh, PA, USA, 2007; Volume 7, pp. 6–9.
5. Huang, L.; Yin, Z.; Wan, Y.; Li, X.; Lu, C. Evaluation and comparison of the gas production potential of the typical four gas hydrate deposits in Shenhu area, South China sea. *Energy* **2020**, *204*, 117955.
6. Ye, J.; Qin, X.; Xie, W.; Lu, H.; Ma, B.; Qiu, H. The second natural gas hydrate production test in the South China Sea. *China Geol.* **2020**, *2*, 197–209. [CrossRef]
7. Xie, Y.F.; Lu, J.A.; Cai, H.M.; Deng, W.; Kuang, Z.G.; Wang, T.; Kang, D.J.; Zhu, C.Q. The in-situ NMR evidence of gas hydrate forming in micro-pores in the Shenhu area, South China Sea. *Energy Rep.* **2022**, *8*, 2936–2946. [CrossRef]
8. Singh, S.C.; Minshull, T.A.; Spence, G.D. Velocity structure of a gas hydrate reflector. *Science* **1993**, *260*, 204–207. [CrossRef]

9. Holbrook, W.S.; Hoskins, H.; Wood, W.T.; Stephen, R.A.; Lizarralde, D. Methane hydrate and free gas on the Blake Ridge from vertical seismic profiling. *Science* **1996**, *273*, 1840–1843. [CrossRef]
10. Hyndman, R.D.; Spence, G.D. A seismic study of methane hydrate marine bottom simulating reflectors. *J. Geophys. Res. Solid Earth* **1992**, *97*, 6683–6698. [CrossRef]
11. Zhang, W.; Liang, J.Q.; Su, P.B.; Wei, J.G.; Hua, G.Y.; Lin, L.; Jin, L.; Wei, H. Distribution and Characteristics of Mud Diapirs, Gas Chimneys, and Bottom Simulating Reflectors Associated with Hydrocarbon Migration and Gas Hydrate Accumulation in the Qiongdongnan Basin, Northern Slope of the South China Sea. *Geol. J.* **2019**, *54*, 3556–3573. [CrossRef]
12. Dai, J.; Xu, H.; Snyder, F.; Dutta, N. Detection and estimation of gas hydrates using rock physics and seismic inversion: Examples from the northern deep-water Gulf of Mexico. *Lead. Edge* **2004**, *23*, 60–66. [CrossRef]
13. Dai, J.; Snyder, F.; Gillespie, D.; Koesoemadinata, A.; Dutta, N. Exploration for gas hydrates in the deepwater, northern Gulf of Mexico: Part I. A seismic approach based on geological model, inversion, and rock physics principles. *Mar. Pet. Geol.* **2008**, *25*, 830–844. [CrossRef]
14. Zhong, G.; Zhang, D.; Zhao, L. Current states of well-logging evaluation of deep-sea gas hydrate-bearing sediments by the international scientific ocean drilling (DSDP/ODP/IODP) programs. *Nat. Gas Ind. B* **2021**, *8*, 128–145. [CrossRef]
15. Zhu, L.Q.; Ma, Y.S.; Cai, J.C.; Zhang, C.M.; Wu, S.G.; Zhou, X.Q. Key factors of marine shale conductivity in southern china—Part I: The influence factors other than the porosity. *J. Pet. Sci. Eng.* **2021**, *205*, 108698. [CrossRef]
16. Zhu, L.Q.; Ma, Y.S.; Cai, J.C.; Zhang, C.M.; Wu, S.G.; Zhou, X.Q. Key factors of marine shale conductivity in southern China—Part II: The influence of pore space and the development direction of shale gas saturation models. *J. Pet. Sci. Eng.* **2022**, *209*, 109516. [CrossRef]
17. Zhou, X.Q.; Zhang, C.; Zhang, Z.S.; Zhang, R.F.; Zhu, L.Q.; Zhang, C.M. A saturation evaluation method in tight gas sandstones based on diagenetic facies. *Mar. Pet. Geol.* **2019**, *107*, 310–325. [CrossRef]
18. Zhu, L.Q.; Zhang, C.M.; Zhang, Z.S.; Zhou, X.Q. High-precision calculation of gas saturation in organic shale pores using an intelligent fusion algorithm and a multi-mineral model. *Adv. Geo-Energy Res.* **2020**, *4*, 135–151. [CrossRef]
19. Archie, G.E. The electrical resistivity log as an aid in determining some reservoir characteristics. *Trans. AIME* **1942**, *146*, 54–62. [CrossRef]
20. Mungan, N.; Moore, E.J. Certain wettability effects on electrical resistivity in porous media. *J. Can. Petrol. Technol.* **1968**, *7*, 20–25. [CrossRef]
21. Lei, D.W.; Tang, Y.; Chang, Q.S. The deep and relatively high-quality clastic reservoir bodies and favorable exploration areas in the southern margin of junggar basin. *Xinjiang Pet. Geol.* **2008**, *29*, 435–438.
22. Spangenberg, E. Modeling of the influence of gas hydrate content on the electrical properties of porous sediments. *J. Geophys. Res. Solid Earth* **2001**, *106*, 6535–6548. [CrossRef]
23. Chen, Q.; Wu, N.; Liu, C.; Zou, C.; Yang, L.; Sun, J.; Li, Y.; Hu, G. Research Progress on Global Marine Gas Hydrate Resistivity Logging and Electrical Property Experiments. *J. Mar. Sci. Eng.* **2022**, *10*, 645. [CrossRef]
24. Waxman, M.H.; Thomas, E.C. Saturation modeling: Using the Waxman-Smits Model/Equation in saturation determination in dispersed shaly sands. *J. Multidiscip. Eng. Sci. Technol.* **2016**, *3*, 4985–4992.
25. Hu, X.D.; Zou, C.C. Application of HB model in hydrate saturation evaluation in frozen soil area of Qilian Mountain. In Proceedings of the Annual Meeting of China Geoscience Federation, Beijing, China, 15–18 October 2017; pp. 521–522.
26. Wang, X.J.; Wu, S.G.; Lee, M.; Guo, Y.Q.; Yang, S.X.; Liang, J.Q. Gas hydrate saturation from acoustic impedance and resistivity logs in the Shenhu area, South China Sea. *Mar. Pet. Geol.* **2011**, *28*, 1625–1633. [CrossRef]
27. Zhao, J.; Shi, Z.F.; Li, Y.P.; Xiang, X.R.; Li, J.; Wei, N. Simulation of conductivity characteristics of gas hydrate reservoirs and its saturation calculation. *Nat. Gas. Geosci.* **2021**, *32*, 1261–1269.
28. Kang, D.J.; Liang, J.Q.; Kuang, Z.G.; Lu, J.A.; Guo, Y.Q.; Liang, J.; Cai, H.M.; Qu, C.W. Application of element capture energy spectrum logging in evaluation of natu-ral gas hydrate reservoir in Shenhu sea area. *Nat. Gas Ind.* **2018**, *38*, 54–60.
29. Chen, G.Q.; Li, C.F.; Liu, C.L.; Xing, L.C. Effect of microscopic distribution of methane hydrate on resistivity in porous media. *Adv. New Renew. Energy* **2019**, *7*, 493–499.
30. Lee, M.W.; Hutchinson, D.R.; Dillon, W.P. Method of estimating the amount of in situ gas hydrates in deep marine sediments. *Mar. Petrol. Geol.* **1993**, *10*, 493–506. [CrossRef]
31. Guerin, G.; Goldberg, D.; Meltser, A. Characterization of in situ elastic properties of gas hydrate-bearing sediments on the Blake Ridge. *J. Geophys. Res.* **1999**, *104*, 17781–17795. [CrossRef]
32. Yadav, U.S.; Shukla, K.M.; Ojha, M.; Kumar, P.; Shankar, U. Assessment of gas hydrate accumulations using velocities derived from vertical seismic profiles and acoustic log data in Krishna-Godavari Basin, India. *Mar. Petrol. Geol.* **2019**, *108*, 551–561. [CrossRef]
33. Freedman, R.; Minh, C.C.; Gubelin, G. Combining NMR and density logs for petrophysical analysis in gas-bearing formations. In Proceedings of the Society of Petrophysicists and Well-Log Analysts 39th Annual Logging Symposium, Keystone, CO, USA, 26–28 May 1998.
34. Li, Y.L.; Liu, L.L.; Jin, Y.R.; Wu, N.Y. Characterization and development of natural gas hydrate in marine clayey-silt reservoirs: A review and discussion. *Adv. Geo-Energy Res.* **2021**, *5*, 75–86. [CrossRef]

35. Sherif, F.; Souvik, S.; Shib, S.G.; Fayez, A.; Mohamed, A.; Khaled, A.K.; Priyantan, G. An integrated petrographical, petrophysical and organic geochemical characterization of the Lower Turonian Abu Roash-F carbonates, Abu Gharadig field, Egypt–Inferences on self-sourced unconventional reservoir potential. *Mar. Pet. Geol.* **2022**, *145*, 105885.
36. Wang, D.D.; Ning, F.L.; Lu, J.A.; Kang, D.J.; Xie, Y.F.; Li, J.; Sun, J.X.; Ou, W.J.; Liu, Z.C.; Fang, B.; et al. Reservoir characteristics and critical influencing factors on gas hydrate accumulations in the Shenhu area, South China Sea. *Mar. Pet. Geol.* **2021**, *133*, 105238. [CrossRef]
37. Sha, Z.B.; Liang, J.Q.; Zhang, G.X.; Yang, S.X.; Lu, J.A.; Zhang, Z.J.; McConnell, D.R.; Humphrey, G. A seepage gas hydrate system in the northern South China Sea: Seismic and well log interpretations. *Mar. Geol.* **2015**, *366*, 69–78. [CrossRef]
38. Yang, S.; Liang, J.; Lu, J.G.; Qu, C.; LiU, B. New understandings on characteristics and controlling factors of gas hydrate reservoirs in Shenhu area on the northern slope of the South China Sea. *Earth Sci. Front.* **2017**, *24*, 1–14.
39. Yang, S.; Zhang, M.; Liang, J. Preliminary results of China's third gas hydrate drilling expedition: A critical step from discovery to development in the South China Sea. *Fire Ice* **2015**, *15*, 1–5.
40. Ge, X.M.; Zeng, B.D.; Li, N.; Xu, H.J.; Liu, H.T.; Gu, D.N.; Sun, W.M.; Fan, Y.R. NMR saturation index and its application to fluid saturation estimation. *J. China Univ. Pet. Ed. Nat. Sci.* **2021**, *45*, 64–72.
41. Kang, D.J.; Lu, J.A.; Zhang, Z.J.; Liang, J.Q.; Kuang, Z.J.; Lu, C.; Kou, B.B.; Lu, Q.P.; Wang, J.L. Fine-grained gas hydrate reservoir properties estimated from well logs and lab measurements at the Shenhu gas hydrate production test site, the northern slope of the South China Sea. *Mar. Pet. Geol.* **2020**, *122*, 104676. [CrossRef]